Journal of Sound and Vibration 329 (2010) 2177–2192

Contents lists available at ScienceDirect

Journal of Sound and Vibration

journal homepage: www.elsevier.com/locate/jsvi

Stability analyses of a vertical axis automatic washing machine without balancer

Hai-Wei Chen *, Qiu-Ju Zhang

School of Mechanical Engineering, Jiangnan University, No.1800 LiHu Road, Wuxi 214122, Jiangsu Province, People's Republic of China

ARTICLE INFO

Article history:
Received 12 July 2009
Received in revised form
23 October 2009
Accepted 6 December 2009
Handling Editor: L.G. Tham
Available online 31 December 2009

ABSTRACT

This paper analyzes the nonlinear vibration characteristics associated with the spin drying process of a vertical axis automatic washing machine without any balancer. At first, damping properties born with the machine's suspension system are discussed and a mathematical model involving tangential damping forces is built. Based on a rotating coordinate transformation, this model is then converted to an autonomous form for stability analyses. The continuation and bifurcation software AUTO [1] is applied and a Hopf bifurcation phenomenon is observed from a one-parameter bifurcation diagram. Based on several two-parameter bifurcation diagrams, several parameters affecting the Hopf bifurcation are then discussed. At last, bifurcation results are validated by time responses of the autonomous system. For a further view of the spin drying process, simulations of the non-autonomous system are also provided. This paper provides a new insight into the spin drying process of the vertical axis automatic washing machine.

1. Introduction

Automatic washing machines may be classified into three types: drum-type, agitator-type and pulsator-type. Drum-type washers have horizontal axes while agitator-type and pulsator-type washers have vertical ones. The agitator-type and the pulsator-type employ different suspension schemes. The former uses bottom mount suspension: the washing/spinning assembly connects directly to a base structure through spring/damper elements; the later uses top mount suspension: the washing/spinning assembly is suspended from four suspension rods.

The working process of an automatic washing machine may be divided into three successive steps: washing, rinsing and spin drying. In the first two steps, imbalance may be created in the basket if clothes clump together. Due to a high ration speed of the basket, the imbalance may cause serious vibrations in the spin drying process. Because of noise and safety requirements, low vibration has become one of the most important performance characteristics of a washing machine. Therefore studies on the dynamics and vibration control principles have attracted lots of attention from researchers and washing machine producers. A detailed review of these studies was conducted by Conrad [2] in his doctoral thesis. The literature obtained was separated into four areas, they are suspension dynamics, walk characteristics, dynamic balancing and clothes loading. He concluded that the area of washing machine design based on dynamic constraints was still in the reserach stage. An introduction of studies on the dynamics of the drum-type and aigtator-type washers was made by Bae et al. [3] in their research paper. After the introduction, they carried out an analytical study on the dynamics of the pulsator-type washing machines.

* Corresponding author. Tel.: +86 15961705236.
E-mail address: chenhaiwei8012@163.com (H.-W. Chen).

0022-460X/$ - see front matter © 2009 Elsevier Ltd. All rights reserved.
doi:10.1016/j.jsv.2009.12.012

A vertical automatic washing machine of pulsator-type is what we will discuss in this paper. In the spin drying process of the pulsator-type washing machine, a hydraulic balancer is often used for vibration suppression. It is partially filled with liquid and attached at the upper part of the basket. At the steady state of the spin drying process, if the ration speed of the basket is high enough, the liquid in the balancer will redistribute and rush to the opposite side of the imbalance under the effect of the centrifugal forces, thus reducing excessive vibrations of the washing machine.

From the literature available, research on the spin drying process of the pulsator-type washing machine may be divided into two categories: the first focuses on the suspension system, such as discussing the effect of air in the damping tub of a suspension rod [4] and suggesting a flexible model for the rod [5]; the other category focuses on the hydraulic balancer, for instance, Bae et al. [3] built a mathematical model to illustrate the distribution of liquid in the hydraulic balancer at the steady state while Wang [6] used three balls to simulate the balancer's effect.

The hydraulic balancer is effective in reducing vibrations of the spin drying process in the steady state; however, due to its nonlinearities, it may increase the imbalance in the transient stage. Based on our simulations, nonlinear vibration properties exist in the spin drying process even without the hydraulic balancer. Although there have been a number of studies on the dynamics of the pulsator-type washing machine, stability analyses of the spin drying process have not yet been reported. In this paper, a mathematical model involving tangential damping forces of the suspension system is built and transformed to an autonomous form for stability analyses. A Hopf bifurcation phenomenon is observed and the influential factors are investigated. In order to investigate basic properties of the spin drying process, a hydraulic balancer is not considered in our mathematical model.

2. Mathematical model

The structure of the vertical-axis automatic washing machine discussed in this paper is shown in Fig. 1(a). This consists of a cabinet, a suspension system and a washing/spinning assembly. The washing/spinning assembly is composed of a hydraulic balancer, a tub, a basket, a motor and a clutch. The assembly is connected to the cabinet through a suspension system with four suspension rods whose structures are shown in Fig. 1(b). The suspension rod contains two spherical joints, a rod and a damping tub. During the spin drying process, the suspension rod can swing and stretch simultaneously, thus both tangential and axial damping forces could be exited.

Three basic assumptions are made in this paper:

(1) The cabinet is fixed to the ground.
(2) The washing/spinning assembly is free to move, no collisions with the cabinet occur during simulations.
(3) All the machine's components can be treated as rigid bodies.

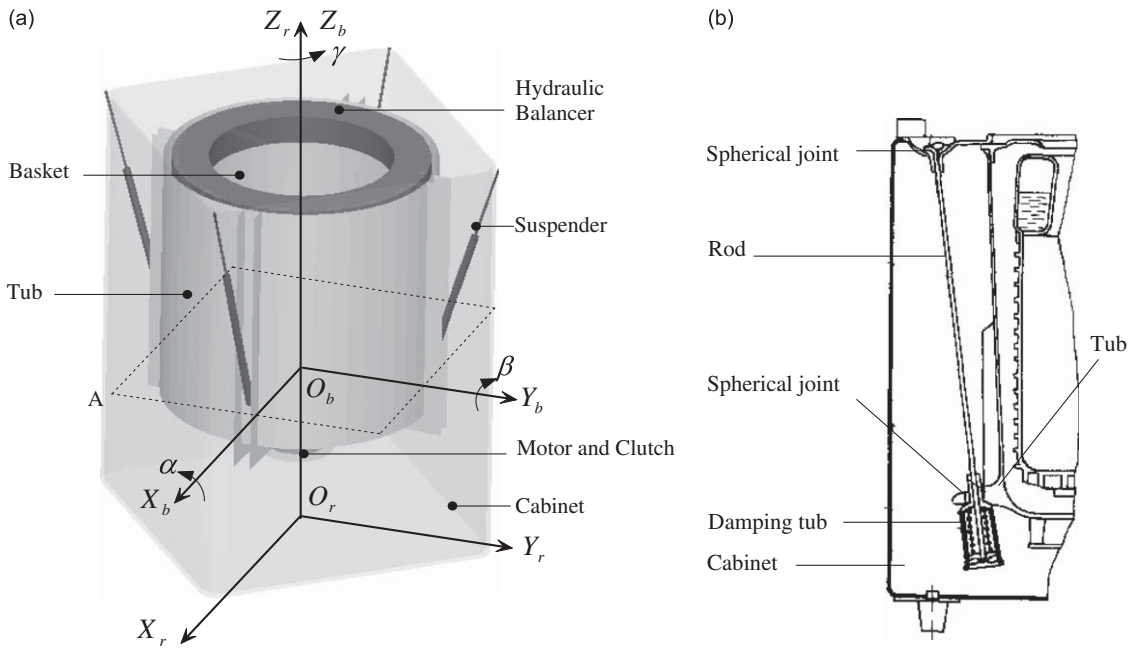

Fig. 1. (a) Structure of a vertical axis automatic washing machine and (b) structure of the suspension system.

2.1. Kinetic energy of the washing/spinning assembly

2.1.1. Reference frames and structure analysis

For describing movements of the washing/spinning assembly, two reference frames are established in Fig. 1(a): a ground reference frame $X_rY_rZ_r$ and a local reference frame $X_bY_bZ_b$ embedded in the tub. It is assumed that the lower spherical joints of the four suspension rods are arranged on plane A which is perpendicular to the vertical axis of the tub (Z_b-axis) with intersection point O_b (the origin of $X_bY_bZ_b$).

For the convenience of calculating the kinetic energy, bodies are classified into two categories: bodies in the first one are fixed on the tub, such as the tub itself, stator of the motor and so on; bodies in the other can rotate around an axis parallel to the vertical axis of the tub, such as the basket, rotator of the motor and clumped clothes.

2.1.2. Kinetic energy of a body in the first category

For obtaining the kinetic energy of a body in the first category, both translational and rotational velocities of the body have to be calculated at first. Assume a body's mass center can be represented by C whose position vector can be denoted by $\mathbf{r}_c$ in $X_bY_bZ_b$. Note that $\mathbf{r}_c$ is constant since a body in this category is fixed on the tub. However, because the body moves along with the tub, the position vector of C in the global reference frame $X_rY_rZ_r$ varies and can be described as

$$\mathbf{s}=\mathbf{x}+\mathbf{A}^{rb}\mathbf{r}_c \tag{1}$$

where $\mathbf{x}=[x\ y\ z]^{\mathrm{T}}$ is the position vector of O_b; $\mathbf{A}^{rb}$ is the transformation matrix from $X_bY_bZ_b$ to $X_rY_rZ_r$ and can be expressed as

$$\mathbf{A}^{rb}=\begin{bmatrix}\cos\beta\cos\gamma & -\cos\beta\sin\gamma & \sin\beta\\ \sin\alpha\sin\beta\cos\gamma+\cos\alpha\sin\gamma & -\sin\alpha\sin\beta\sin\gamma+\cos\alpha\cos\gamma & -\sin\alpha\cos\beta\\ -\cos\alpha\sin\beta\cos\gamma+\sin\alpha\sin\gamma & \cos\alpha\sin\beta\sin\gamma+\sin\alpha\cos\gamma & \cos\alpha\cos\beta\end{bmatrix} \tag{2}$$

where $\{\alpha\ \ \beta\ \ \gamma\}$ are Cardan's angles. Now, we discuss the body's translational velocity. Differentiating Eq. (1) with respect to time yields

$$\dot{\mathbf{s}}=\dot{\mathbf{x}}+\dot{\mathbf{A}}^{rb}\mathbf{r}_c=\dot{\mathbf{x}}+\mathbf{A}^{rb}\widetilde{\boldsymbol{\omega}_b}\,\mathbf{r}_c=\dot{\mathbf{x}}-\mathbf{A}^{rb}\widetilde{\mathbf{r}_c}\boldsymbol{\omega}_b \tag{3}$$

with $\boldsymbol{\omega}_b$ the angular velocity of $X_bY_bZ_b$ (expressed in $X_bY_bZ_b$) which can be expressed as

$$\boldsymbol{\omega}_b=\mathbf{B}\dot{\boldsymbol{\varphi}} \tag{4}$$

where $\dot{\boldsymbol{\varphi}}=[\dot\alpha\ \ \dot\beta\ \ \dot\gamma]^{\mathrm{T}}$ is the derivative of Cardan's angles; $\mathbf{B}$ is the transformation matrix relating $\boldsymbol{\omega}_b$ to $\dot{\boldsymbol{\varphi}}$ and can be described as

$$\mathbf{B}=\begin{bmatrix}\cos\beta\cos\gamma & \sin\gamma & 0\\ -\cos\beta\sin\gamma & \cos\gamma & 0\\ \sin\beta & 0 & 1\end{bmatrix}. \tag{5}$$

After substituting Eq. (4) into Eq. (3), the body's translational velocity can be expressed as

$$\dot{\mathbf{s}}=\dot{\mathbf{x}}-\mathbf{A}^{rb}\widetilde{\mathbf{r}_c}\mathbf{B}\ \dot{\boldsymbol{\varphi}}=[\mathbf{I}_3\quad -\mathbf{A}^{rb}\widetilde{\mathbf{r}_c}\mathbf{B}]\dot{\mathbf{q}} \tag{6}$$

where $\mathbf{I}_3$ is a 3×3 identity matrix and $\dot{\mathbf{q}}=[\dot x\ \dot y\ \dot z\ \dot\alpha\ \dot\beta\ \dot\gamma]^{\mathrm{T}}$. We now calculate the body's angular velocity. Considering each body has its individual reference frame which can be denoted by $X_cY_cZ_c$, the body's angular velocity can be expressed in $X_cY_cZ_c$ as

$$\boldsymbol{\omega}_c=(\mathbf{A}^{bc})^{\mathrm{T}}\boldsymbol{\omega}_b=(\mathbf{A}^{bc})^{\mathrm{T}}\mathbf{B}\,\dot{\boldsymbol{\varphi}}=[\mathbf{0}_{3\times3}\ \ (\mathbf{A}^{bc})^{\mathrm{T}}\mathbf{B}]\dot{\mathbf{q}} \tag{7}$$

where $\mathbf{A}^{bc}$ is the transformation matrix from $X_cY_cZ_c$ to $X_bY_bZ_b$ ($\mathbf{A}^{bc}$ is a constant matrix for a body in the first category); $\mathbf{0}_{3\times3}$ represents a 3×3 zero matrix. The body's kinetic energy can be expressed as

$$T=\frac{1}{2}m\dot{\mathbf{s}}^{\mathrm{T}}\dot{\mathbf{s}}+\frac{1}{2}\boldsymbol{\omega}_c^{\mathrm{T}}\mathbf{J}_c\boldsymbol{\omega}_c \tag{8}$$

where m is the body's mass and $\mathbf{J}_c$ is the body's inertia tensors. The body's kinetic energy can be further described after substituting Eqs. (6) and (7) into Eq. (8) as

$$\begin{aligned}T&=\frac{1}{2}m\dot{\mathbf{q}}^{\mathrm{T}}\begin{bmatrix}\mathbf{I}_3\\ -\mathbf{B}^{\mathrm{T}}(\widetilde{\mathbf{r}_c})^{\mathrm{T}}(\mathbf{A}^{rb})^{\mathrm{T}}\end{bmatrix}[\mathbf{I}_3\ \ -\mathbf{A}^{rb}\widetilde{\mathbf{r}_c}\mathbf{B}]\dot{\mathbf{q}}+\frac{1}{2}\dot{\mathbf{q}}^{\mathrm{T}}\begin{bmatrix}\mathbf{0}_{3\times3}\\ \mathbf{B}^{\mathrm{T}}\mathbf{A}^{bc}\end{bmatrix}\mathbf{J}_c[\mathbf{0}_{3\times3}\ \ (\mathbf{A}^{bc})^{\mathrm{T}}\mathbf{B}]\dot{\mathbf{q}}\\ &=\frac{1}{2}\dot{\mathbf{q}}^{\mathrm{T}}\begin{bmatrix}m\mathbf{I}_3 & -m\mathbf{A}^{rb}\widetilde{\mathbf{r}_c}\mathbf{B}\\ -m(\mathbf{A}^{rb}\widetilde{\mathbf{r}_c}\mathbf{B})^{\mathrm{T}} & \mathbf{B}^{\mathrm{T}}(m(\widetilde{\mathbf{r}_c})^{\mathrm{T}}\widetilde{\mathbf{r}_c}+(\mathbf{A}^{bc})\mathbf{J}_c(\mathbf{A}^{bc})^{\mathrm{T}})\mathbf{B}\end{bmatrix}\dot{\mathbf{q}}\end{aligned} \tag{9}$$

2.1.3. Kinetic energy of a body in the second category

We now calculate kinetic energy of a body in the second category. A body in the second category can rotate around an axis parallel to the Z_b-axis. Assume a body's mass center can be represented by C whose position can be expressed in $X_bY_bZ_b$ as

$$\mathbf{r}_c = \mathbf{p} + \mathbf{u} \tag{10}$$

where $\mathbf{p} = [p_x \;\; p_y \;\; p_z]^{\mathrm{T}}$ is a constant vector with p_x and p_y describing the position of the body's rotation axis and p_z representing the height of C; $\mathbf{u}$ is a variable vector which can be expressed as

$$\mathbf{u} = [R_u \cos\theta_c \;\; R_u \sin\theta_c \;\; 0]^{\mathrm{T}} \tag{11}$$

where R_u is the radius of gyration and θ_c is the rotation angle. It should be noted that both $\mathbf{p}$ and $\mathbf{u}$ are measured in $X_bY_bZ_b$. Considering movements of the tub, the position vector of C can be described in $X_rY_rZ_r$ as

$$\mathbf{s} = \mathbf{x} + \mathbf{A}^{rb}\,\mathbf{r}_c = \mathbf{x} + \mathbf{A}^{rb}(\mathbf{p} + \mathbf{u}) \tag{12}$$

We now calculate the body's translational velocity. This can be obtained by differentiating Eq. (12) with respect to time

$$\dot{\mathbf{s}} = \dot{\mathbf{x}} + \dot{\mathbf{A}}^{rb}(\mathbf{p} + \mathbf{u}) + \mathbf{A}\dot{\mathbf{u}} = \dot{\mathbf{x}} - \mathbf{A}^{rb}(\widetilde{\mathbf{p} + \mathbf{u}})\mathbf{B}\dot{\phi} + \mathbf{A}^{rb}\frac{\partial \mathbf{u}}{\partial \theta_c}\dot{\theta}_c = \left[\mathbf{I}_3 \quad -\mathbf{A}^{rb}\widetilde{\mathbf{r}}_c\mathbf{B} \quad \mathbf{A}^{rb}\frac{\partial \mathbf{u}}{\partial \theta_c}\right]\dot{\boldsymbol{\kappa}}_c \tag{13}$$

where $\dot{\boldsymbol{\kappa}}_c = [\dot{x} \;\; \dot{y} \;\; \dot{z} \;\; \dot{\alpha} \;\; \dot{\beta} \;\; \dot{\gamma} \;\; \dot{\theta}_c]^{\mathrm{T}}$. We now calculate the body's angular velocity which can be expressed in its individual reference frame $X_cY_cZ_c$ as

$$\boldsymbol{\omega}_c = (\mathbf{A}^{bc})^{\mathrm{T}}(\boldsymbol{\omega}_b + \mathbf{e}\dot{\theta}_c) = (\mathbf{A}^{bc})^{\mathrm{T}}\mathbf{B}\dot{\phi} + (\mathbf{A}^{bc})^{\mathrm{T}}\mathbf{e}\dot{\theta}_c = [\mathbf{0}_{3\times 3} \;\; (\mathbf{A}^{bc})^{\mathrm{T}}\mathbf{B} \;\; (\mathbf{A}^{bc})^{\mathrm{T}}\mathbf{e}]\dot{\boldsymbol{\kappa}}_c \tag{14}$$

where $\mathbf{e} = \begin{bmatrix} 0 & 0 & 1 \end{bmatrix}^{\mathrm{T}}$ describes the direction of the body's rotation axis in $X_bY_bZ_b$and $\mathbf{A}^{bc}$ represents the transformation matrix from the body's reference frame to $X_bY_bZ_b$. $\mathbf{A}^{bc}$ can be expressed as

$$\mathbf{A}^{bc} = \begin{bmatrix} \cos\theta_c & -\sin\theta_c & 0 \\ \sin\theta_c & \cos\theta_c & 0 \\ 0 & 0 & 1 \end{bmatrix} \tag{15}$$

Note that $(\mathbf{A}^{bc})^{\mathrm{T}}\mathbf{e} = \mathbf{e}$, the body's kinetic energy can be obtained after substituting Eqs. (13), (14) into Eq. (8)

$$T = \dot{\boldsymbol{\kappa}}_c^{\mathrm{T}} \begin{bmatrix} m\mathbf{I}_3 & -m\mathbf{A}^{rb}\widetilde{\mathbf{r}}_c\mathbf{B} & m\mathbf{A}^{rb}\dfrac{\partial \mathbf{u}}{\partial \theta_c} \\ -m(\mathbf{A}^{rb}\widetilde{\mathbf{r}}_c\mathbf{B})^{\mathrm{T}} & \mathbf{B}^{\mathrm{T}}(m(\widetilde{\mathbf{r}}_c)^{\mathrm{T}}\widetilde{\mathbf{r}}_c + (\mathbf{A}^{bc})\mathbf{J}_c(\mathbf{A}^{bc})^{\mathrm{T}})\mathbf{B} & \mathbf{B}^{\mathrm{T}}\left(-m(\widetilde{\mathbf{r}}_c)^{\mathrm{T}}\dfrac{\partial \mathbf{u}}{\partial \theta_c} + (\mathbf{A}^{bc})\mathbf{J}_c\mathbf{e}\right) \\ m\left(\mathbf{A}^{rb}\dfrac{\partial \mathbf{u}}{\partial \theta_c}\right)^{\mathrm{T}} & \left(-m(\widetilde{\mathbf{r}}_c)^{T}\dfrac{\partial \mathbf{u}}{\partial \theta_c} + (\mathbf{A}^{bc})\mathbf{J}_c\mathbf{e}\right)^{\mathrm{T}}\mathbf{B} & m\left(\dfrac{\partial \mathbf{u}}{\partial \theta_c}\right)^{\mathrm{T}}\left(\dfrac{\partial \mathbf{u}}{\partial \theta_c}\right) + \mathbf{e}^{\mathrm{T}}\mathbf{J}_c\mathbf{e} \end{bmatrix} \dot{\boldsymbol{\kappa}}_c \tag{16}$$

where

$$\frac{\partial \mathbf{u}}{\partial \theta_c} = \begin{bmatrix} -R_u \sin\theta_c & R_u \cos\theta_c & 0 \end{bmatrix}^{\mathrm{T}} \tag{17}$$

2.1.4. Kinetic energy of the washing/spinning assembly

We now calculate the kinetic energy of the washing/spinning assembly. This can be obtained by adding all the bodies' kinetic energies together. Assume that the basket's rotational speed can be represented by $\dot{\theta}$, the rotational speed of the ith body in the second category can be expressed as $\dot{\theta}_{ci} = p_i\dot{\theta}$ where p_i is a constant proportional coefficient (p_i=1 for the basket). It is assumed that there areN_1bodies in the first category and N_2bodies in the second one, total kinetic energy of the assembly can be expressed as

$$T_{\mathbb{R}} = \sum_{i=1}^{N} T_i = \frac{1}{2}\dot{\boldsymbol{\kappa}}^{\mathrm{T}}\mathbf{M}_{\mathbb{R}}\dot{\boldsymbol{\kappa}} \tag{18}$$

where $N=N_1+N_2$; $\dot{\boldsymbol{\kappa}}=[\dot{x}\quad \dot{y}\quad \dot{z}\quad \dot{\alpha}\quad \dot{\beta}\quad \dot{\gamma}\quad \dot{\theta}]^{\mathrm{T}}$;

$$\mathbf{M}_{\mathbb{R}}=\begin{bmatrix} \left(\sum_{i=1}^{N} m_i\right)\mathbf{I}_3 & -\mathbf{A}^{rb}\left(\sum_{i=1}^{N} m_i\widetilde{\mathbf{r}_{ci}}\right)\mathbf{B} & \mathbf{A}^{rb}\left(\sum_{j=1}^{N_2} m_j p_j \dfrac{\partial \mathbf{u}_j}{\partial\theta_{cj}}\right) \\ -\left(\mathbf{A}^{rb}\left(\sum_{i=1}^{N} m_i\widetilde{\mathbf{r}_{ci}}\right)\mathbf{B}\right)^{\mathrm{T}} & \mathbf{B}^{\mathrm{T}}\left(\sum_{i=1}^{N} m_i(\widetilde{\mathbf{r}_{ci}})^{\mathrm{T}}\widetilde{\mathbf{r}_{ci}}+(\mathbf{A}_i^{bc})\mathbf{J}_{ci}(\mathbf{A}_i^{bc})^{\mathrm{T}}\right)\mathbf{B} & \mathbf{B}^{\mathrm{T}}\sum_{j=1}^{N_2}\left(-m_j p_j(\widetilde{\mathbf{r}_{cj}})^{\mathrm{T}}\dfrac{\partial \mathbf{u}_j}{\partial\theta_{cj}}+p_j(\mathbf{A}_j^{bc})\mathbf{J}_{cj}\mathbf{e}\right) \\ \left(\mathbf{A}^{rb}\left(\sum_{j=1}^{N_2} m_j p_j \dfrac{\partial \mathbf{u}_j}{\partial\theta_{cj}}\right)\right)^{\mathrm{T}} & \left(\sum_{j=1}^{N_2}\left(-m_j p_j(\widetilde{\mathbf{r}_{cj}})^{\mathrm{T}}\dfrac{\partial \mathbf{u}_j}{\partial\theta_{cj}}+p_j(\mathbf{A}_j^{bc})\mathbf{J}_{cj}\mathbf{e}\right)\right)^{\mathrm{T}}\mathbf{B} & \sum_{j=1}^{N_2}\left(m_j p_j^2\left(\dfrac{\partial \mathbf{u}_j}{\partial\theta_{cj}}\right)^{\mathrm{T}}\left(\dfrac{\partial \mathbf{u}_j}{\partial\theta_{cj}}\right)+p_j^2\mathbf{e}^{\mathrm{T}}\mathbf{J}_{cj}\mathbf{e}\right) \end{bmatrix} \tag{19}$$

where $\mathbf{e}=[0\quad 0\quad 1]^{\mathrm{T}}$.

2.2. Geopotential energy of the washing/spinning assembly

We now calculate the geopotential energy of the washing/spinning assembly. Assume that the mass of the ith body can be represented by m_i, the body's geopotential energy can be described as

$$V_{gi}=m_i g s_{zi} \tag{20}$$

where g is the local gravitational acceleration; s_{zi} is the third component of the vector "**s**" defined in Eqs. (1) (12) and can be expressed as

$$s_{zi}=z+\mathbf{A}_{3,:}^{rb}\mathbf{r}_{ci} \tag{21}$$

with $\mathbf{A}_{3,:}^{rb}$ representing all the elements in the third row of $\mathbf{A}^{rb}$. We now calculate the total geopotential energy of the washing/spinning assembly. This can be obtained by adding all the bodies' geopotential energy together, such that

$$V_g=\left[\sum_{i=1}^{N} m_i(z+\mathbf{A}_{3,:}^{rb}\mathbf{r}_{ci})\right]g \tag{22}$$

where N represents the number of bodies in the washing/spinning assembly.

2.3. Generalized forces provided by the suspension system

This section discusses generalized forces provided by the suspension system. Considering the mass of the suspension rod is very small, inertia forces acting on it can be neglected. We now establish a local reference frame denoted by $\mathbf{e}_1-\mathbf{e}_2-\mathbf{e}_3$ for a suspension rod, see Fig. 2. Assume that the position vector of the suspension rod's lower spherical joint O can be represented by $\mathbf{r}_d$ in $X_bY_bZ_b$. Considering movements of the tub, the position vector of joint$O$ can be expressed

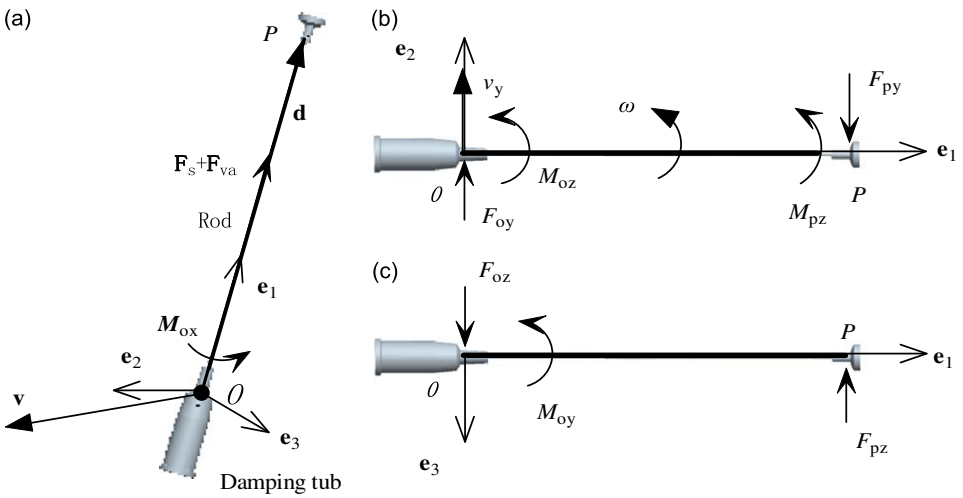

Fig. 2. Forces acting on a suspension rod: (a) direction vectors and forces along $\mathbf{e}_1$; (b) tangential damping forces in plane $\mathbf{e}_1-O-\mathbf{e}_2$ and (c) tangential damping forces in plane $\mathbf{e}_3-O-\mathbf{e}_1$.

in $X_rY_rZ_r$ as

$$\mathbf{s}_d = \mathbf{x} + \mathbf{A}^{rb}\mathbf{r}_d \tag{23}$$

We now calculate the translational velocity at O. This can be obtained by differentiating the above equation with respect to time

$$\mathbf{v} = \dot{\mathbf{x}} - \mathbf{A}^{rb}\tilde{\mathbf{r}}_d\mathbf{B}\dot{\boldsymbol{\phi}} \tag{24}$$

Now we discuss the vector $\mathbf{d}$ displayed in Fig. 2(a). Assume that the position vector of the suspension rod's upper spherical joint P can be denoted by $\mathbf{s}_u$ in $X_rY_rZ_r$, the vector $\mathbf{d}$ in Fig. 2(a) can be derived as

$$\mathbf{d} = \mathbf{s}_u - \mathbf{s}_d = \mathbf{s}_u - \mathbf{x} - \mathbf{A}^{rb}\mathbf{r}_d \tag{25}$$

where $\mathbf{s}_d$ was described in Eq. (23). Now let

$$\mathbf{t} = \mathbf{d} \times \mathbf{v} \tag{26}$$

the following three normalized direction vectors orthogonal to each other can be obtained

$$\mathbf{e}_1 = \mathbf{d}/\mathbf{d} \tag{27}$$

$$\mathbf{e}_3 = \mathbf{t}/\mathbf{t} \tag{28}$$

$$\mathbf{e}_2 = \mathbf{e}_3 \times \mathbf{e}_1 \tag{29}$$

The local reference frame $\mathbf{e}_1 - \mathbf{e}_2 - \mathbf{e}_3$ can be constructed based on these vectors.

2.3.1. Forces along the direction $\boldsymbol{e}_1$

The forces along the direction $\mathbf{e}_1$ are shown in Fig. 2(a). Two forces act on the suspension rod along the direction $\mathbf{e}_1$: one is the restoring force of the spring and the other is the axial damping force provided by the damping tub. The restoring force can be described as

$$F_s = -K_s(|\mathbf{d}| - l_0) \tag{30}$$

With K_s the stiffness of the spring and l_0 the initial length of the rod that outsides the damping tub. The axial damping force can be expressed as

$$F_{va} = -C_a(-\mathbf{v}\cdot\mathbf{e}_1) = C_a(\mathbf{v}\cdot\mathbf{e}_1) \tag{31}$$

with C_a representing the axial damping coefficient of the suspension rod.

2.3.2. Tangential damping forces in plane $\boldsymbol{e}_1 - O - \boldsymbol{e}_2$

The tangential damping forces in plane $\mathbf{e}_1 - O - \mathbf{e}_2$ are shown in Fig. 2(b), they are excited by angular velocities of the suspension rod and the tub. First, we derive the torque at joint P. Considering translational velocity at point O along the direction $\mathbf{e}_2$ is

$$v_y = \mathbf{v}\cdot\mathbf{e}_2 \tag{32}$$

angular velocity of the suspension rod in plane $\mathbf{e}_1 - O - \mathbf{e}_2$ can be described as

$$\omega = -v_y/\mathbf{d} \tag{33}$$

Viscous damping is assumed in joints and the torque aroused byωat joint P can be described as

$$M_{pz} = -C_p\omega \tag{34}$$

Where C_p is the damping coefficient of joint P. Now, we calculate the torque at the spherical joint O. In order to do this, the angular velocity of tub described in Eq. (4) needs to be expressed in $X_rY_rZ_r$ as

$$\boldsymbol{\omega}_b^r = \mathbf{A}^{rb}\,\boldsymbol{\omega}_b = \mathbf{A}^{rb}\mathbf{B}\dot{\boldsymbol{\phi}} \tag{35}$$

Considering Eqs. (33)(35), the torque due to damping at the spherical joint O can be derived as

$$M_{oz} = -C_{oz}(\omega - \boldsymbol{\omega}_b^r\cdot\mathbf{e}_3) \tag{36}$$

Where C_{oz} is the damping coefficient of joint O along the direction $\mathbf{e}_3$. Now, we discuss the force acting on joint O. Considering the following equilibrium condition in plane $\mathbf{e}_1 - O - \mathbf{e}_2$ has to be satisfied

$$M_{pz} + M_{oz} - F_{oy}|\mathbf{d}| = 0 \tag{37}$$

the force acting on joint O along the direction $\mathbf{e}_2$ can be derived as

$$F_{oy} = \frac{M_{pz} + M_{oz}}{|\mathbf{d}|} \tag{38}$$

2.3.3. Tangential damping forces in plane $\mathbf{e}_3-O-\mathbf{e}_1$

We now discuss tangential damping forces in plane $\mathbf{e}_3-O-\mathbf{e}_1$ which are excited by angular velocities of the tub, see Fig. 2(c). Considering the angular velocity of the tub in plane $\mathbf{e}_3-O-\mathbf{e}_1$ is $\boldsymbol{\omega}_b^r\cdot\mathbf{e}_2$, the torque acting on joint O along the direction $\mathbf{e}_2$ can be described as

$$M_{oy}=-C_{oy}(0-\boldsymbol{\omega}_b^r\cdot\mathbf{e}_2)=C_{oy}(\boldsymbol{\omega}_b^r\cdot\mathbf{e}_2) \tag{39}$$

Where C_{oy} is the damping coefficient of joint O along the direction $\mathbf{e}_2$. Because the following equilibrium condition has to be satisfied in plane $\mathbf{e}_3-O-\mathbf{e}_1$

$$F_{oz}|\mathbf{d}|+M_{oy}=0 \tag{40}$$

the force acting on joint O along the direction $\mathbf{e}_3$ can be derived as

$$F_{oz}=-\frac{M_{oy}}{|\mathbf{d}|} \tag{41}$$

2.3.4. Tangential damping forces in plane $\mathbf{e}_2-O-\mathbf{e}_3$

We now calculate damping forces in plane $\mathbf{e}_2-O-\mathbf{e}_3$, this can be calculated with the assumption that the suspension rod can not rotate around $\mathbf{e}_1$. Considering the angular velocity of the tub along $\mathbf{e}_1$ is $\boldsymbol{\omega}_b^r\cdot\mathbf{e}_1$, the torque acting on O along the direction $\mathbf{e}_1$ can be described as

$$M_{ox}=-C_{ox}(0-\boldsymbol{\omega}_b^r\cdot\mathbf{e}_1)=C_{ox}(\boldsymbol{\omega}_b^r\cdot\mathbf{e}_1) \tag{42}$$

with C_{ox} the damping coefficient of joint O along the direction $\mathbf{e}_1$.

2.3.5. Generalized forces provided by the suspension system

Axial damping forces and restoring forces of the springs were calculated in Section 2.3.1. Tangential damping forces and torques were discussed in Sections 2.3.2 to 2.3.4. We now calculate generalized forces provided by the suspension system. For doing this, we have to get the resultant force and torque at first, and then project the resultant force and torque on the generalized coordinates.

First, we calculate the resultant force acting on joint O, this can be obtained by adding all the forces along directions $\mathbf{e}_1$, $\mathbf{e}_2$, and $\mathbf{e}_3$ together. The resultant force acting on joint O can be expressed as

$$\mathbf{F}_o=(F_s+F_{va})\mathbf{e}_1+F_{oy}\mathbf{e}_2+F_{oz}\mathbf{e}_3 \tag{43}$$

where F_s is the restoring force of the spring discussed in Eq. (30); F_{va} is the axial damping force described in Eq. (31); F_{oy} is the tangential damping force along the direction $\mathbf{e}_2$ described in Eq. (38); F_{oz} is the tangential damping force along the direction $\mathbf{e}_3$ expressed in Eq. (41).

We now calculate the resultant torque acting on joint O, this can be obtained by adding all the torques along directions $\mathbf{e}_1$, $\mathbf{e}_2$ and $\mathbf{e}_3$ together. The resultant torque acting on joint O can be expressed as

$$\mathbf{M}_o=M_{ox}\mathbf{e}_1+M_{oy}\mathbf{e}_2+M_{oz}\mathbf{e}_3 \tag{44}$$

where M_{ox} is the tangential damping torque in plane $\mathbf{e}_2-O-\mathbf{e}_3$ expressed in Eq. (42); M_{oy} is the tangential damping torque in plane $\mathbf{e}_3-O-\mathbf{e}_1$ described in Eq. (39);M_{oz} is the tangential damping torque in plane $\mathbf{e}_1-O-\mathbf{e}_2$ discussed in Eq. (36).

It should be noted that the generalized forces are provided by the reaction forces of the resultant force $\mathbf{F}_o$ and the result torque $\mathbf{M}_o$. In other words, the generalized forces are provided by $-\mathbf{F}_o$ and $-\mathbf{M}_o$ that act on the tub.

We now project $-\mathbf{F}_o$ and $-\mathbf{M}_o$ on the generalized coordinates. The generalized forces provided by the ith suspension rod can be expressed as

$$\mathbf{Q}_i=-\begin{bmatrix}\mathbf{F}_o\\ (\mathbf{A}^{rb}\mathbf{B})^{\mathrm{T}}(\mathbf{M}_o+\widetilde{\mathbf{A}^{rb}\mathbf{r}_d}\mathbf{F}_o)\end{bmatrix} \tag{45}$$

where $\mathbf{r}_d$ is the position vector of joint O which was described in $X_bY_bZ_b$.

We now calculate generalized forces provided the suspension system. This can be obtained by adding all the generalized forces provided by the four suspension rods together. Total generalized forces can be expressed as

$$\mathbf{Q}=\sum_{i=1}^{4}\mathbf{Q}_i \tag{46}$$

where $\mathbf{Q}_i$ is the generalized forces provided by the ith suspension rod.

2.4. Vibration model of the system

Kinetic energy of the system was discussed in Section 2.1 and described in Eq. (18). Geopotential energy of the system was introduced in Section 2.2 and described in Eq. (22). Generalized forces provided by the suspension system was studied

in Section 2.3 and described in Eq. (46). This section discusses the vibration model of the system. This can be obtained by substituting the kinetic energy, geopotential energy and generalized forces into Lagrange's equation. The derived vibration model of the system can be expressed as

$$\mathbf{M}_{\mathbb{R}}\ddot{\boldsymbol{\kappa}}=\frac{1}{2}\left[\frac{\partial\mathbf{M}_{\mathbb{R}}}{\partial\boldsymbol{\kappa}}\dot{\boldsymbol{\kappa}}\right]^{\mathrm{T}}\dot{\boldsymbol{\kappa}}-\dot{\mathbf{M}}_{\mathbb{R}}\dot{\boldsymbol{\kappa}}+\begin{bmatrix}\mathbf{Q}\\0\end{bmatrix}-\frac{\partial V_g}{\partial\boldsymbol{\kappa}} \tag{47}$$

where $\boldsymbol{\kappa}=[x\ \ y\ \ z\ \ \alpha\ \ \beta\ \ \gamma\ \ \theta]^{\mathrm{T}}$ represents the generalized coordinates; $\mathbf{M}_{\mathbb{R}}$is the mass matrix described in Eq. (19); $\mathbf{Q}$ is the generalized force described in Eq. (46); $\partial V_g/\partial\boldsymbol{\kappa}$ is the partial derivatives of the geopotential energy V_g.

It should be noted that, during simulations, because rotations of the basket θ are given, the governing equation on θ needs to be removed from Eq. (47). After the removing, the following governing equations on coordinates $\{x\ \ y\ \ z\ \ \alpha\ \ \beta\ \ \gamma\}$ are derived

$$\mathbf{M}\ddot{\mathbf{q}}=\frac{1}{2}\left[\frac{\partial\mathbf{M}}{\partial\mathbf{q}}\dot{\mathbf{q}}\right]^{\mathrm{T}}\dot{\mathbf{q}}-\dot{\mathbf{M}}\dot{\mathbf{q}}+\mathbf{F}(\dot{\theta},\ddot{\theta})+\mathbf{Q}-\frac{\partial V_g}{\partial\mathbf{q}} \tag{48}$$

where $\mathbf{q}=[x\ y\ z\ \alpha\ \beta\ \gamma]^{\mathrm{T}}$,

$$\mathbf{M}=\begin{bmatrix}\left(\sum_{i=1}^{N}m_i\right)\mathbf{I}_3 & -\mathbf{A}^{rb}\left(\sum_{i=1}^{N}m_i\widetilde{\mathbf{r}_{ci}}\right)\mathbf{B}\\ -\left(\mathbf{A}^{rb}(\sum_{i=1}^{N}m_i\widetilde{\mathbf{r}_{ci}})\mathbf{B}\right)^{\mathrm{T}} & \mathbf{B}^{\mathrm{T}}\left(\sum_{i=1}^{N}m_i(\widetilde{\mathbf{r}_{ci}})^{\mathrm{T}}\widetilde{\mathbf{r}_{ci}}+(\mathbf{A}_i^{bc})\mathbf{J}_{ci}(\mathbf{A}_i^{bc})^{\mathrm{T}}\right)\mathbf{B}\end{bmatrix} \tag{49}$$

and $\mathbf{F}(\dot{\theta},\ddot{\theta})$ represents elements relevant to $\dot{\theta}$ or $\ddot{\theta}$ which can be expressed as

$$\mathbf{F}(\dot{\theta},\ddot{\theta})=\left[\dot{\mathbf{q}}^{\mathrm{T}}\frac{\partial\boldsymbol{\Gamma}}{\partial\mathbf{q}}\right]^{\mathrm{T}}\dot{\theta}-\left(\sum_{i=1}^{6}\frac{\partial\boldsymbol{\Gamma}}{\partial q_i}\dot{q}_i\right)\dot{\theta}-\left(\frac{\partial\boldsymbol{\Gamma}}{\partial\theta}\dot{\theta}\right)\dot{\theta}-\left(\frac{\partial\mathbf{M}}{\partial\theta}\dot{\theta}\right)\dot{\mathbf{q}}-\boldsymbol{\Gamma}\ddot{\theta} \tag{50}$$

with

$$\boldsymbol{\Gamma}=\begin{bmatrix}\mathbf{A}^{rb}\left(\sum_{j=1}^{N_2}m_jp_j\frac{\partial\mathbf{u}_j}{\partial\theta_{cj}}\right)\\ \mathbf{B}^{\mathrm{T}}\sum_{j=1}^{N_2}\left(-m_jp_j(\widetilde{\mathbf{r}_{cj}})^{\mathrm{T}}\frac{\partial\mathbf{u}_j}{\partial\theta_{cj}}+p_j(\mathbf{A}_j^{bc})\mathbf{J}_{cj}\mathbf{e}\right)\end{bmatrix} \tag{51}$$

2.5. Autonomous equations in a rotating reference frame

We now discuss an autonomous form in a rotating reference frame. The autonomous form is necessary for performing stability analyses. A method similar to that described in [7] is employed to convert Eq. (48) to an autonomous form in a rotating reference frame with constant angular velocity Ω ($\Omega=\dot{\theta}$). First, the following substitutions are considered

$$\begin{aligned}\tau&=\Omega t\\ \frac{\mathrm{d}\tau}{\mathrm{d}t}&=\Omega\\ x&=\varepsilon_1\cos(\tau)-\varepsilon_2\sin(\tau)\\ y&=\varepsilon_1\sin(\tau)+\varepsilon_2\cos(\tau)\\ z&=\varepsilon_3\\ \alpha&=\varepsilon_4\cos(\tau)-\varepsilon_5\sin(\tau)\\ \beta&=\varepsilon_5\sin(\tau)+\varepsilon_5\cos(\tau)\\ \gamma&=\varepsilon_6\end{aligned} \tag{52}$$

We now express the above substitutions in a matrix–vector form:

$$\mathbf{q}=\mathbf{H}\boldsymbol{\varepsilon} \tag{53}$$

where

$$\mathbf{H}=\begin{bmatrix}\cos(\tau) & -\sin(\tau) & 0 & 0 & 0 & 0\\ \sin(\tau) & \cos(\tau) & 0 & 0 & 0 & 0\\ 0 & 0 & 1 & 0 & 0 & 0\\ 0 & 0 & 0 & \cos(\tau) & -\sin(\tau) & 0\\ 0 & 0 & 0 & \sin(\tau) & \cos(\tau) & 0\\ 0 & 0 & 0 & 0 & 0 & 1\end{bmatrix} \tag{54}$$

$\mathbf{q}$ is the generalized coordinates $\mathbf{q}=[x \quad y \quad z \quad \alpha \quad \beta \quad \gamma]^{\mathrm{T}}$; $\boldsymbol{\varepsilon}=\begin{bmatrix}\varepsilon_1 & \varepsilon_2 & \varepsilon_3 & \varepsilon_4 & \varepsilon_5 & \varepsilon_6\end{bmatrix}^{\mathrm{T}}$.

We now express the generalized velocities $\dot{\mathbf{q}}$ and generalized accelerations $\ddot{\mathbf{q}}$ as functions of $\boldsymbol{\varepsilon}$, $\dot{\boldsymbol{\varepsilon}}$ and $\ddot{\boldsymbol{\varepsilon}}$. Generalized velocities of the original system can be derived by differentiating Eq. (53) with respect to time

$$\dot{\mathbf{q}}=\dot{\mathbf{H}}\boldsymbol{\varepsilon}+\mathbf{H}\dot{\boldsymbol{\varepsilon}} \tag{55}$$

and generalized accelerations can be derived after a further differentiation of the above equation with respect to time

$$\ddot{\mathbf{q}}=\ddot{\mathbf{H}}\boldsymbol{\varepsilon}+2\dot{\mathbf{H}}\dot{\boldsymbol{\varepsilon}}+\mathbf{H}\ddot{\boldsymbol{\varepsilon}} \tag{56}$$

We now derive the autonomous formulation. This can be obtained after substituting the generalized coordinates $\mathbf{q}$ in Eq. (53), generalized velocities $\dot{\mathbf{q}}$ in Eq. (55) and generalized accelerations $\ddot{\mathbf{q}}$ in Eq. (56) into the original system Eq. (48)

$$\mathbf{M}\mathbf{H}\ddot{\boldsymbol{\varepsilon}}=\mathbf{G}(\boldsymbol{\varepsilon},\dot{\boldsymbol{\varepsilon}})-\mathbf{M}\ddot{\mathbf{H}}\boldsymbol{\varepsilon}-2\mathbf{M}\dot{\mathbf{H}}\dot{\boldsymbol{\varepsilon}} \tag{57}$$

where

$$\mathbf{G}(\boldsymbol{\varepsilon},\dot{\boldsymbol{\varepsilon}})=\frac{1}{2}\left[\frac{\partial\mathbf{M}}{\partial\mathbf{q}}\dot{\mathbf{q}}\right]^{\mathrm{T}}\dot{\mathbf{q}}-\dot{\mathbf{M}}\dot{\mathbf{q}}+\mathbf{F}(\dot{\theta},\ddot{\theta})+\mathbf{Q}-\frac{\partial V_g}{\partial\mathbf{q}} \tag{58}$$

Let $\dot{\boldsymbol{\varepsilon}}=\mathbf{z}$, the above system can be transformed into a first-order formulation which is necessary for stability analyses

$$\begin{cases}\dot{\boldsymbol{\varepsilon}}=\mathbf{z}\\ \dot{\mathbf{z}}=(\mathbf{M}\mathbf{H})^{-1}(\mathbf{G}(\boldsymbol{\varepsilon},\mathbf{z})-\mathbf{M}\ddot{\mathbf{H}}\boldsymbol{\varepsilon}-2\mathbf{M}\dot{\mathbf{H}}\mathbf{z})\end{cases} \tag{59}$$

We now discuss the equilibrium point of the autonomous form. Considering $\dot{\boldsymbol{\varepsilon}}=\mathbf{0}$ and $\dot{\mathbf{z}}=\ddot{\boldsymbol{\varepsilon}}=\mathbf{0}$ at the equilibrium point, the point has the following form:

$$\xi^*=\begin{bmatrix}\boldsymbol{\varepsilon}^*\\ \mathbf{z}^*\end{bmatrix}=\begin{bmatrix}\boldsymbol{\varepsilon}^*\\ \mathbf{0}\end{bmatrix} \tag{60}$$

where $\mathbf{z}^*=\dot{\boldsymbol{\varepsilon}}^*=\mathbf{0}$. Substituting $\dot{\boldsymbol{\varepsilon}}=0$, $\ddot{\boldsymbol{\varepsilon}}=\dot{\mathbf{z}}=\mathbf{0}$ into Eq. (57) yields

$$\boldsymbol{\psi}=\mathbf{G}(\boldsymbol{\varepsilon}^*)-\mathbf{M}\ddot{\mathbf{H}}\boldsymbol{\varepsilon}^*=\mathbf{0} \tag{61}$$

For getting $\boldsymbol{\varepsilon}^*$, Newton–Raphson method is employed

$$\boldsymbol{\varepsilon}^*_{n+1}=\boldsymbol{\varepsilon}^*_n-\mathbf{J}_{\psi}^{-1}\boldsymbol{\psi}(\boldsymbol{\varepsilon}^*_n) \tag{62}$$

where

$$\mathbf{J}_{\psi}=\frac{\partial\mathbf{G}}{\partial\boldsymbol{\varepsilon}}-\frac{\partial\mathbf{M}}{\partial\boldsymbol{\varepsilon}}\ddot{\mathbf{H}}\boldsymbol{\varepsilon}-\mathbf{M}\ddot{\mathbf{H}} \tag{63}$$

with

$$\frac{\partial\mathbf{G}}{\partial\boldsymbol{\varepsilon}}=\frac{\partial\mathbf{G}}{\partial\mathbf{q}}\mathbf{H}+\frac{\partial\mathbf{G}}{\partial\dot{\mathbf{q}}}\dot{\mathbf{H}} \tag{64}$$

and

$$\frac{\partial\mathbf{M}}{\partial\boldsymbol{\varepsilon}}=\frac{\partial\mathbf{M}}{\partial\mathbf{q}}\mathbf{H} \tag{65}$$

3. Discussions

3.1. Stability analyses

Numerical bifurcation theory, specifically the continuation and bifurcation software AUTO [1] is employed here to analyze the stability of the equilibrium point described in Section 2.5. An imbalance mass representing the clothes is considered and fixed on the basket. The mass, radius of gyration and height of the imbalance are denoted by m_u, R_u, and h_u (measured in $X_bY_bZ_b$), respectively. Values of the tangential damping coefficients described in Section 2.3 are assumed to be the same, namely $C_{ox}=C_{oy}=C_{oz}=C_p$. Table 1 shows parameters used in the analyses, including their nominal values,

Table 1
Parameters for analyses.

Parameters	Note	Nominal value	Lower limit	Upper limit	Unit
Imbalance mass	m_u	1	0	2.5	kg
Gyration radius of the imbalance	R_u	0.15	0	0.25	m
Rotational speed of the basket	Ω	10	0	15	Hz
Axial damping coefficient of the suspension system	C_a	100	0	5000	$N\,s\,m^{-1}$
Stiffness coefficient of the suspension system	K_s	1800	500	4500	$N\,s\,m^{-1}$

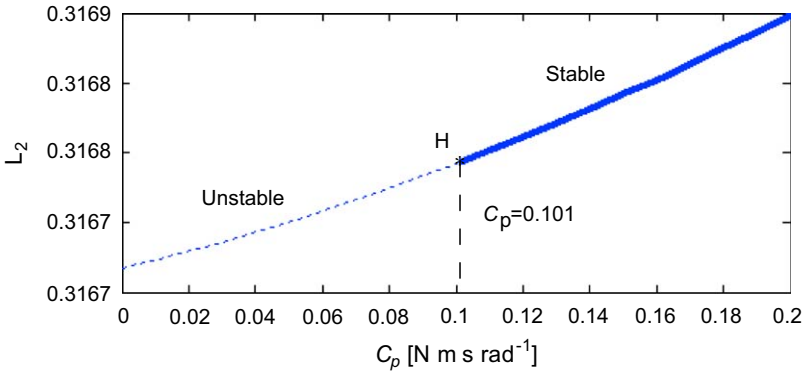

Fig. 3. One parameter bifurcation diagrams showing variations of the tangential damping coefficient $C_p(C_{ox}=C_{oy}=C_{oz}=C_p)$. A Hopf bifurcation H is indicated by a (*). Thick curve means the equilibrium point is stable while dot curve means unstable. The ordinate L_2 represents the default norm used by AUTO.

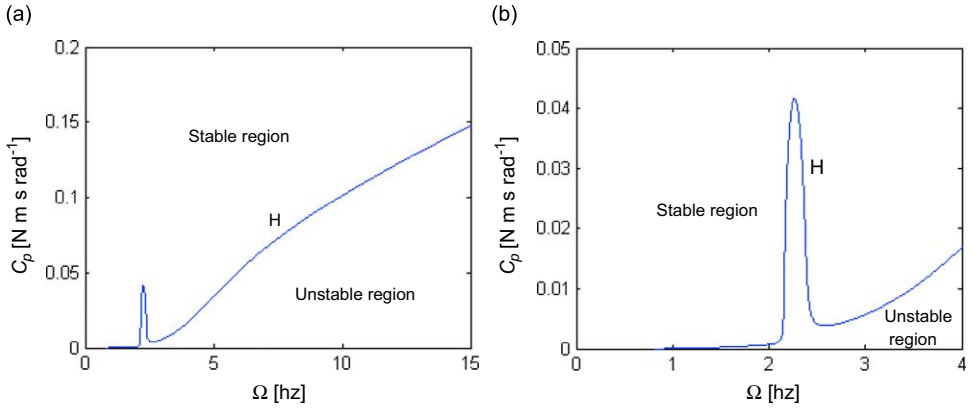

Fig. 4. Two-parameter bifurcation diagrams showing variations of the rotational speed of the basket Ω and the tangential damping coefficient R_u. H represents the curve of the Hopf bifurcation.

lower limits and upper limits. During the analyses, the height of the imbalance is assumed to be $h_u=0.1$ m. Newton–Raphson method is used to get the initial equilibrium position of the autonomous form based on which bifurcation analyses are carried out in AUTO.

Fig. 3 gives one-parameter bifurcation diagrams showing variations of the tangential damping coefficient $C_p(C_{ox}=C_{oy}=C_{oz}=C_p)$. This paper focuses on the stability of the equilibrium point of the autonomous system introduced in Section 2.5. If the real parts of all the eigenvalues of the autonomous system are negative, the equilibrium point is stable; otherwise, if at least one eigenvalue has positive real part, the equilibrium point is unstable. Hopf bifurcations occur when a pair of pure eigenvalues crosses the imaginary axis; see, for example, Ref. [8]. As can be seen from Fig. 3, along with the increase of the tangential damping coefficient C_p, a Hopf bifurcation phenomenon happens, the equilibrium point changes from unstable to stable. In this paper, a stable equilibrium point implies that the spin drying process has a stable periodic solution.

We now consider parameters affecting the Hopf bifurcation. The five parameters listed in Table 1 are considered. Fig. 4(a) and (b) shows the results of two-parameter bifurcation analyses upon variations of the rotational speed Ω and the tangential damping coefficient C_p. In Fig. 4, H represents the curve of the Hopf bifurcation, it is the boundary curve that separates the stable region from the unstable one. An equilibrium point in the stable region is stable, which implies a

periodic solution of the spin drying process. Each C_p on the bifurcation curve represents a critical tangential damping coefficient. For a specific Ω, in order to keep the spin drying process stable, C_p should be bigger than the critical tangential damping coefficient. As can be seen from Fig. 4, generally speaking, the critical damping coefficient grows bigger as the rotational speed Ω increases. This implies that, in order to keep the spin drying process stable, a higher design value of rotational speed Ω usually requires a larger tangential damping coefficient C_p.

Fig. 5(a)and (b) shows the results of two-parameter bifurcation analyses upon variations of parameters $m_u - C_p$ and $R_u - C_p$, respectively. As can be seen, the critical tangential damping coefficient C_p grows larger when the imbalance mass m_u or the imbalance's gyration radius R_u increases. This means, in order to keep the equilibrium point stable, a higher design value of the load for the washing machine needs a larger tangential damping coefficient. Fig. 5(c) displays the results of two-parameter bifurcation analyses concerning the imbalance mass m_u and the imbalance's gyration radius R_u. We now analyze the relation between R_u and m_u. Let $y = R_u$ and $x = 1/m_u$, an one-degree polynomial is fitted to the data of y and x by a polyfit $(x, y, 1)$ command in *Matlab*. The result shows that the relation between y and x can be described as $y = 0.1387x + 0.0114$. Because $y = R_u$ and $x = 1/m_u$, the relation between $R_u$and m_u can be derived as $R_u = 0.1387/m_u + 0.0114$, which means the imbalance's gyration radius R_u is in inverse proportion to the imbalance mass m_u.

Fig. 6(a) and (b) shows the results of two-parameter bifurcation analyses upon variations of the axial damping coefficient C_a and the tangential damping coefficient C_p. As can be seen, along with the increase of the axial damping coefficient C_a, the critical tangential damping coefficient C_p grows bigger at first in the interval $C_a \in [0, 154]$, and then decreases after $C_a = 154\,\mathrm{N\,m\,s^{-1}}$. According to Fig. 6, it may be reasonable to use a smaller axial damping coefficient C_a to keep the equilibrium point stable since a smaller axial damping coefficient C_a corresponds to a smaller critical tangential damping coefficient C_p in the interval $C_a \in [0.154]$. However, according to our experiments, if the axial damping coefficient C_a is too small, transient vibrations of the washing machine will be extremely serious. In order to keep the spin drying

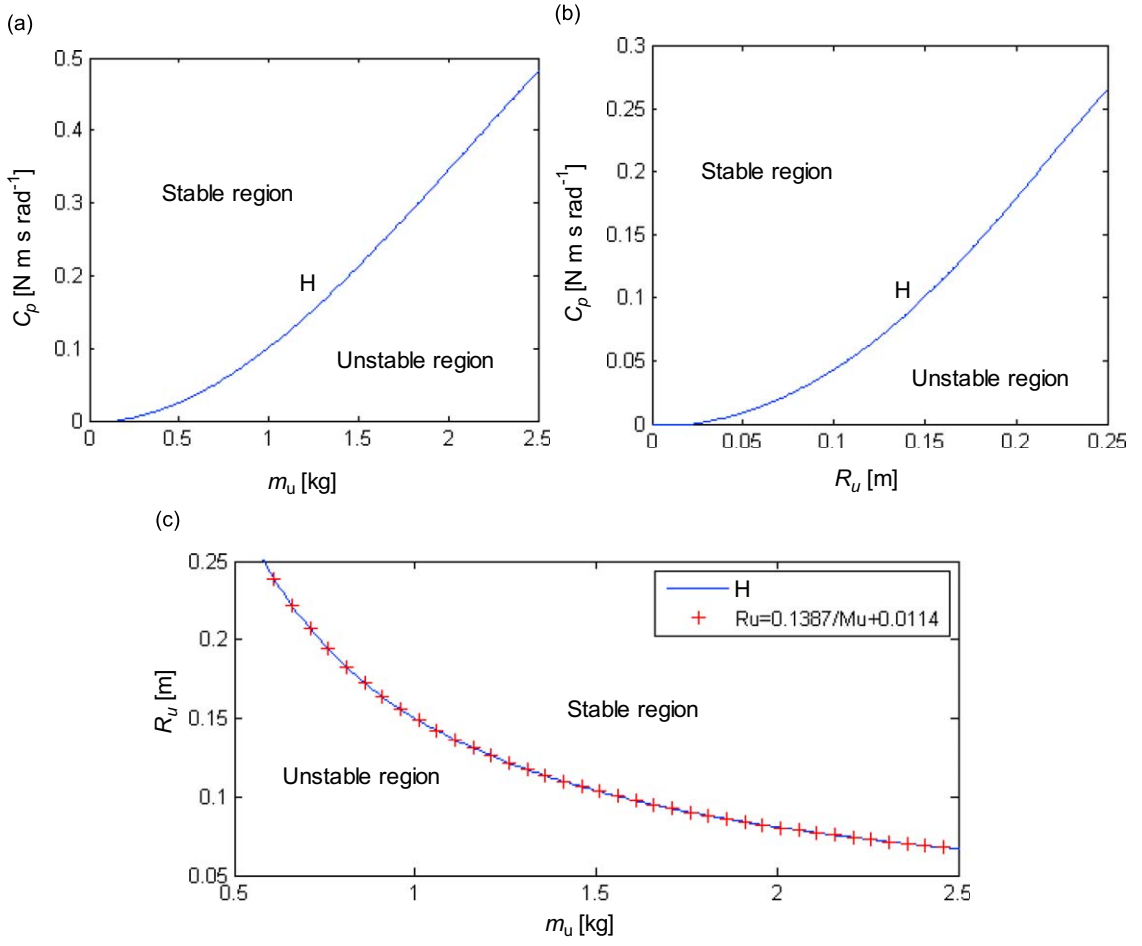

Fig. 5. (a) Two-parameter bifurcation diagrams upon variations of the imbalance mass m_u and the tangential damping coefficient C_p; (b) two-parameter bifurcation diagrams upon variations of the imbalance's gyration radius R_u and the tangential damping coefficient C_p and (c) two-parameter bifurcation diagrams upon variations the imbalance mass m_u and the imbalance's gyration radius R_u.

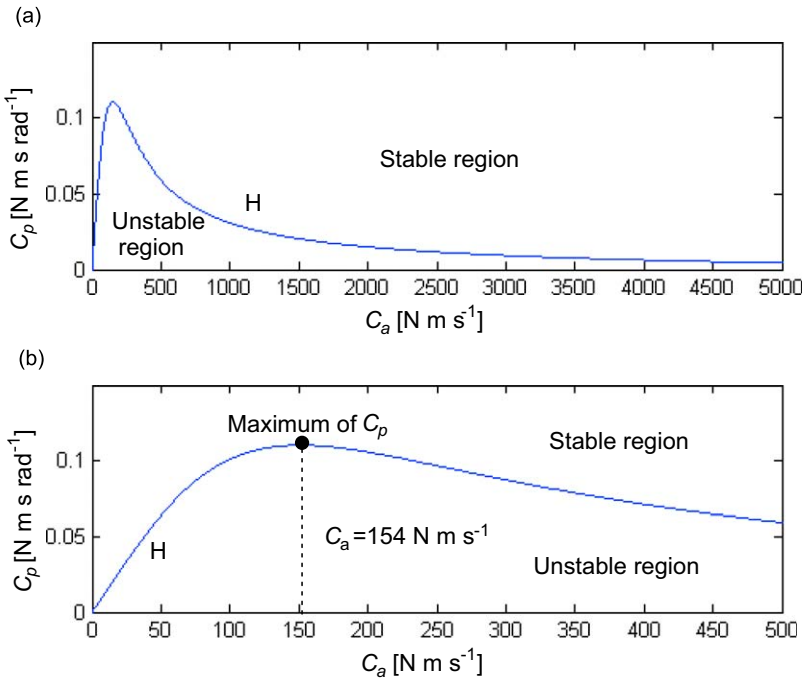

Fig. 6. Two-parameter bifurcation diagrams upon variations of the axial damping coefficient C_a and the tangential damping coefficient C_p.

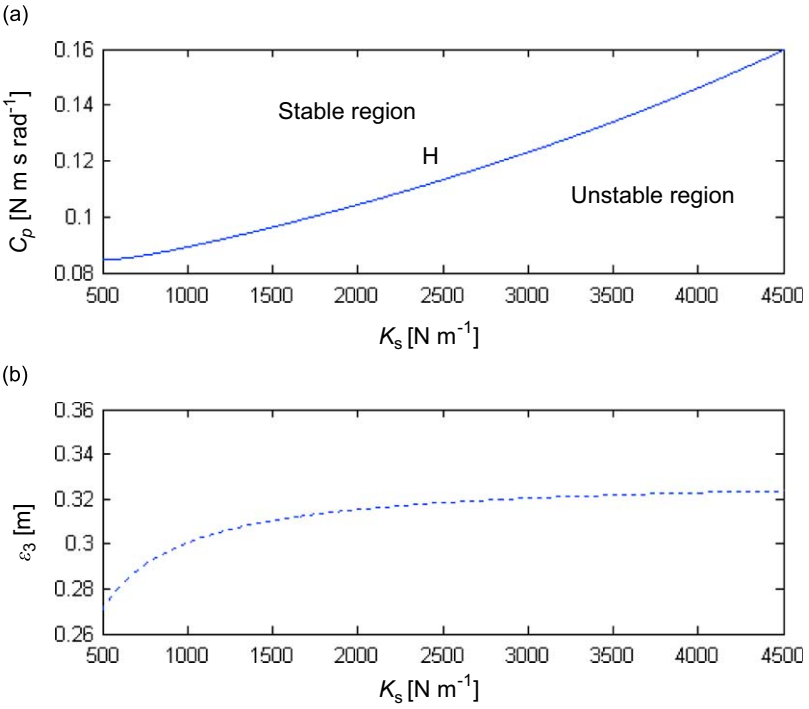

Fig. 7. (a) Two-parameter bifurcation diagrams upon variations of the stiffness coefficient K_s and the tangential damping coefficient C_p and (b) the variations of component ε_3 of the vector $\boldsymbol{\varepsilon}$ in Eq. (53).

process stable, a bigger axial damping coefficient C_a is recommended and a large-enough tangential damping coefficient C_p has to be supplied.

Fig. 7(a) shows the results of two-parameter bifurcation analyses upon variations of the stiffness coefficient of the suspension system $K_s$and the tangential damping coefficient C_p.The figure shows that the critical tangential damping

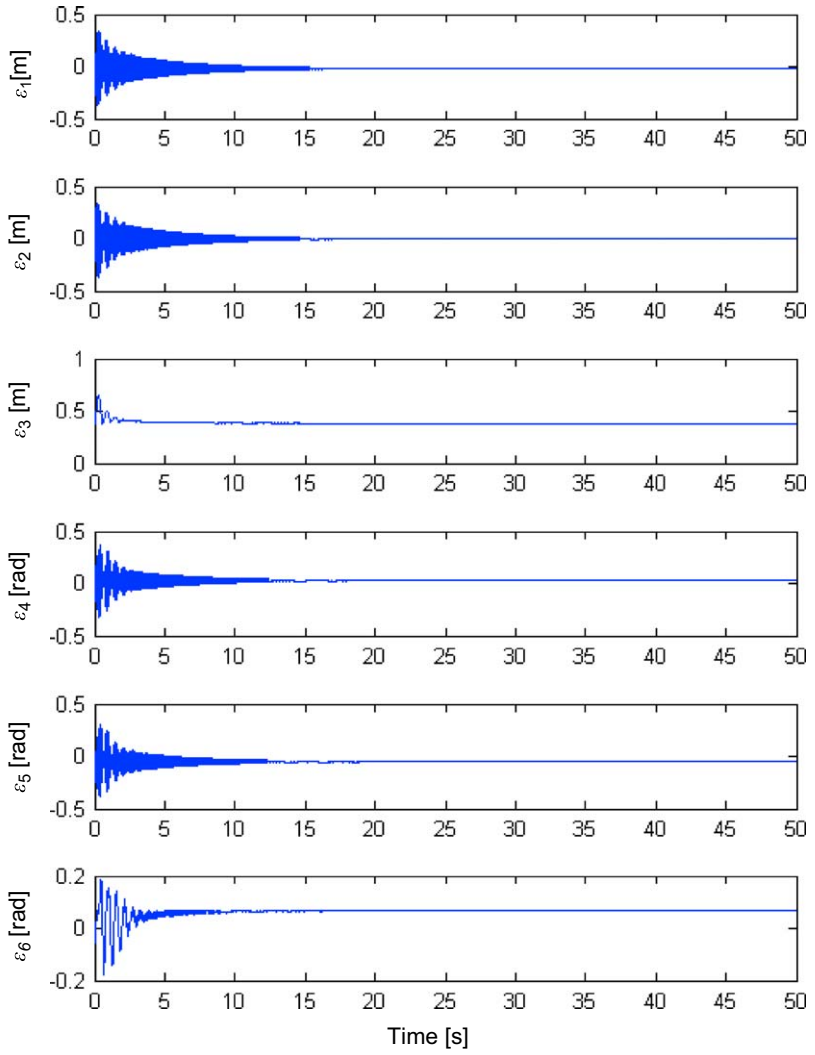

Fig. 8. Numerical simulation for the autonomous system when the tangential damping coefficient $C_p = 0.15\,\mathrm{N\,m\,s\,rad^{-1}}$.

coefficient C_p grows bigger when the stiffness coefficient K_s increases. It can be seen that the interval $K_s \in [0, 500)$ is not included in Fig. 7(a), since if the stiffness coefficient K_s is too small, the deformation of the spring will be too large and the position of the tub in the cabinet will be too low to be accepted, as can be seen from Fig. 7(b).

3.2. Time responses

In order to validate the bifurcation results obtained in Section 3.1, time responses are discussed in this section. First, time responses of the autonomous system described in Eq. (57) are presented with the purpose of validation. Then for a further view of the spin drying process, simulations of the non-autonomous system described in Eq. (48) are provided.

3.2.1. Time responses of the autonomous system

Time responses of the autonomous system described in Eq. (57) are obtained by numerical integration method, specifically the *Matlab routine ode45*. Nominal values of parameters in Table 1 are considered, the height of the imbalance is assumed to be $h_u = 0.1$ m, initial conditions are selected as $\varepsilon_1 = \varepsilon_2 = \varepsilon_4 = \varepsilon_5 = \varepsilon_6 = 0$, $\varepsilon_3 = 0.408$ and $\dot{\boldsymbol{\varepsilon}} = \mathbf{0}$.

Figs. 8 and 9 explore dynamics of the bifurcation curve shown in Fig. 3. According to Fig. 3, the equilibrium point of the autonomous system is stable when the tangential damping coefficient $C_p > 0.101\,\mathrm{N\,m\,s\,rad^{-1}}$ and unstable if $C_p < 0.101\,\mathrm{N\,m\,s\,rad^{-1}}$. Figs. 8 and 9 show simulations of the autonomous system for $C_p = 0.15$ and $C_p = 0\,\mathrm{N\,m\,s\,rad^{-1}}$, respectively. Fig. 8 shows that a fixed solution is achieved after $t \approx 20$ s which implies the equilibrium point is obtained. Fig. 9 shows an oscillatory solution which means the equilibrium point could not be achieved at all. As can be seen from these figures, the equilibrium point of the system is stable when the tangential damping coefficient $C_p = 0.15\,\mathrm{N\,m\,s\,rad^{-1}}$

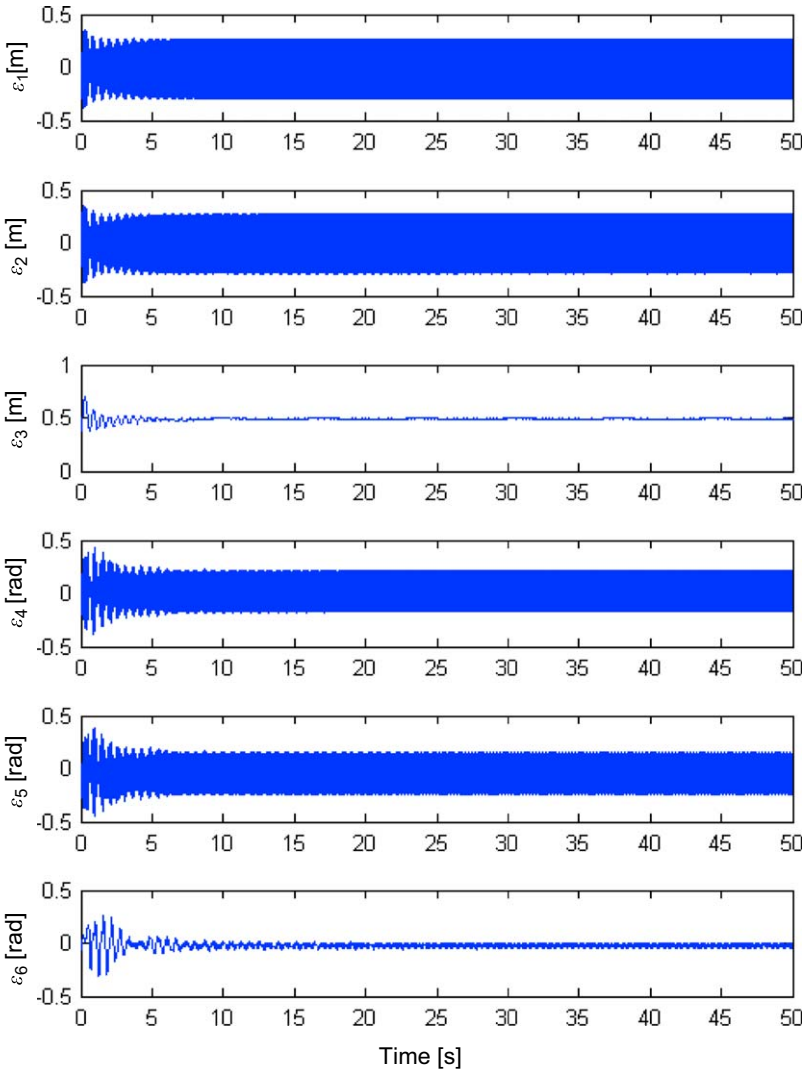

Fig. 9. Numerical simulation for the autonomous system when the tangential damping coefficient $C_p = 0\,\mathrm{N\,m\,s\,rad^{-1}}$.

but unstable when $C_p = 0\,\mathrm{N\,m\,s\,rad^{-1}}$. The results agree with the bifurcation diagrams in Fig. 3. It can be found that at the initial stage, the vibration amplitudes of the six components are quite large. This is because no acceleration phase is considered during the simulations and the rotational acceleration of the basket is extremely large at t=0 s. The acceleration phase will be discussed in the following section.

3.2.2. *Time responses of the non-autonomous system*

Section 3.2.1 showed simulation results of the autonomous system. It can be seen that, when the tangential damping coefficient $C_p > 0.101\,\mathrm{N\,m\,s\,rad^{-1}}$, the equilibrium point of the autonomous system is stable; however, once $C_p < 0.101\,\mathrm{N\,m\,s\,rad^{-1}}$, the equilibrium point is unstable. It should be noted that a stable equilibrium point of the autonomous system corresponds to a stable period solution of the non-autonomous one. This section discusses vibrations of the non-autonomous system at the conditions that $C_p > 0.101\,\mathrm{N\,m\,s\,rad^{-1}}$ and $C_p < 0.101\,\mathrm{N\,m\,s\,rad^{-1}}$ for a further view of the dynamic characteristics the spin drying process.

The relation $\dot{\theta} = \Omega$ was assumed for the autonomous system in the above sections. Because the rotational speed of the basket Ω was assumed to be constant, no acceleration phase was considered in the above sections. This section presents time responses of the non-autonomous system described in Eq. (48). During our simulations, the following acceleration phase is considered

$$\dot{\theta} = \Omega(1 - \mathrm{e}^{-t/\tau}) \tag{66}$$

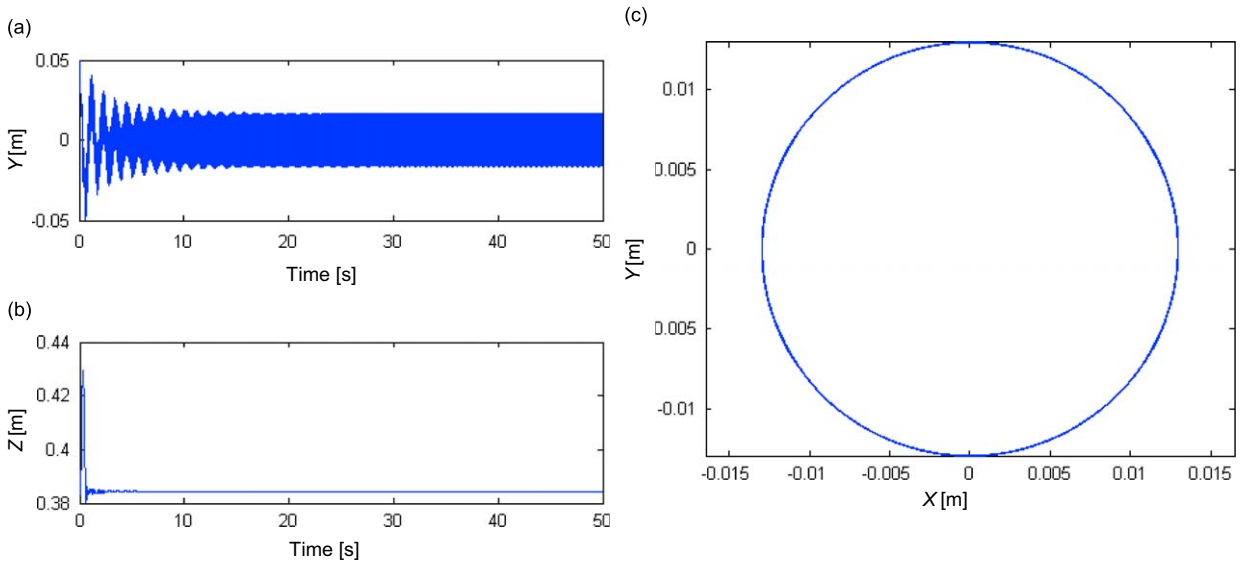

Fig. 10. Time responses of the non-autonomous system when the tangential damping coefficient $C_p = 0.15\,\mathrm{N\,m\,s\,rad^{-1}}$: (a) Y-direction movement of O_b (the original of the dynamic reference frame $X_bY_bZ_b$); (b) Z-direction movement of O_b; (c) trajectory ofO_b projected in plane XY ($t \in [30, 50]$).

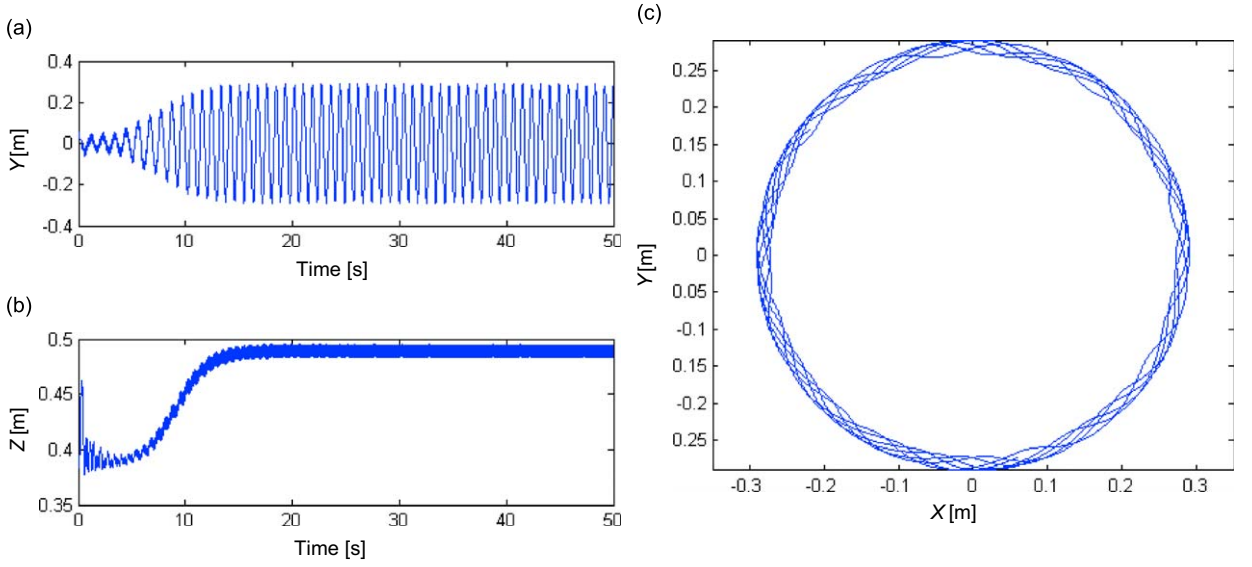

Fig. 11. Time responses of the non-autonomous system when the tangential damping coefficient $C_p = 0\,\mathrm{N\,m\,s\,rad^{-1}}$: (a) Y-direction movement of O_b; (b) Z-direction movement of O_b; (c) trajectory of O_b projected in plane XY ($t \in [45, 50]$).

where Ω is the rotational speed at the final state, and τ is a time constant. Two situations corresponding to C_p=0.15 and $0\,\mathrm{N\,m\,s\,rad^{-1}}$ are considered. Simulations are carried out using *Matlab routine ode45* with parameter values $\Omega = 10\,\mathrm{Hz}$, $\tau = 0.45$, $m_u = 1\,\mathrm{kg}$, $R_u = 0.15\,\mathrm{m}$, $h_u = 0.1\,\mathrm{m}$, $C_a = 100\,\mathrm{N\,s\,m^{-1}}$ and $K_s = 1800\,\mathrm{N\,m^{-1}}$. The initial conditions are selected as $\mathbf{q}^* = [0\ \ 0.05\ \ 0.395\ \ 0.095\ \ 0\ \ 0]^{\mathrm{T}}$, $\dot{\mathbf{q}} = \mathbf{0}$. Here $\mathbf{q}^*$ is the static equilibrium position of the washing machine.

Fig. 10 gives time responses of the non-autonomous system when the tangential damping coefficient $C_p = 0.15\,\mathrm{N\,m\,s\,rad^{-1}}$. As can been seen from Fig. 10(a), the vibration amplitude of O_b (the original of the dynamic reference frame $X_bY_bZ_b$) along the direction Y decreases during the transient stage, and then keeps stable after $t \approx 30$s. Trajectory projection in Fig. 10(c) shows that the movement of O_b trends to a circle which implies a periodic solution.

Fig. 11 shows simulations of the non-autonomous system when the tangential damping coefficient $C_p = 0\,\mathrm{N\,m\,s\,rad^{-1}}$. As can be seen from Fig. 11(a), during the starting stage, the vibration amplitude of O_b (the original of the dynamic reference frame $X_bY_bZ_b$) along the direction Y increases quickly. At the same time, Fig. 11(b) reveals that the position of O_b gets higher and higher. Fig. 11(c) shows the trajectory of O_b projected in plane XY ($t \in [45, 50]$). As can be seen, the vibration amplitude of the system is very large. As the figure shows, more than one frequency exists at the steady state.

For validating or mathematical model, an animation of the instability of spin drying process made by the mechanical system simulation software ADAMS is provided in Appendix A. As can be seen, the animation provides the same results as Fig. 11.

4. Conclusions

A mathematical model involving tangential damping forces of the suspension system was built for a vertical axis automatic washing machine and then converted to an autonomous form for stability analyses. A Hopf bifurcation phenomenon was observed by a variation of the tangential damping coefficient C_p. Parameters affecting the Hopf bifurcation including the rotational speed Ω, mass of the clothes m_u, radius of gyration R_u, axial damping coefficient C_a and spring stiffness K_s were considered. Based on our bifurcation results, the following conclusions can be obtained: ① As the rotational speed Ω, stiffness coefficient K_s, imbalance mass m_u or imbalance's gyration radius R_u increases, a bigger damping coefficient C_p is required; ② The imbalance's gyration radius R_u is in inverse proportion to the imbalance's mass m_u; ③ When the axial damping coefficient C_a increases, the tangential damping coefficient grows bigger a C_p the beginning, and then decreases after its maximum.

Acknowledgement

The authors would like to acknowledge the support provided by the Wuxi LittleSwan Group CO. LTD.

Appendix A. Animation of the instability of the spin drying process

The animation named "Instability of the spin drying process.avi" is made by the mechanical system simulation software ADAMS and describes the instability of the drying process. When the tangential forces are not considered in our mathematical model, namely the tangential damping coefficient C_p=0, the suspension rod can be simplified as a spring–damper. In the virtual prototype of the washing machine, four spring–dampers are used to describe the effect of the suspension system. During the simulation, the following parameters: $\Omega = 10\,\text{Hz}$,$\tau = 0.45$, $m_u = 1\,\text{kg}$,$R_u = 0.15\,\text{m}$, $h_u = 0.1\,\text{m}$, $C_a = 100\,\text{N s m}^{-1}$ and $K_s = 1800\,\text{N m}^{-1}$ are considered. It can be seen from the animation that when the tangential damping coefficient C_p=0, the spin drying process cannot keep stable. This is consistent with our analyses.

Appendix B. Supplementary material

Supplementary data associated with this article can be found in the online version at doi:10.1016/j.jsv.2009.12.012.

References

[1] 〈http://cmvl.cs.concordia.ca/auto/〉.(Accessed 15 June 2009).
[2] D.C. Conrad., The Fundamentals of Automatic Washing Machine Design Based upon Dynamic Constraints[Ph..D., PhD Thesis]., Purdue University, 1994.
[3] S. Bae, J.M. Lee, Y.J. Leekang, et al., Dynamic analysis of an automatic washing machine with a hydraulic balancer, *Journal of Sound and Vibration* 257 (1) (2002) 3–18.
[4] H.W. Chen, Q.J. Zhang, Vibration model for a vertical axis automatic washing machine, *Journal of Vibration and Shock* 27 (1) (2008) 159–162,166.
[5] H.W. Chen, Q.J. Zhang., G.F. Su, A rigid-flexible coupling vibration model for a vertical axis automatic washing machine, *Proceedings of ICMEM2007* „ Science Press, USA Inc.2007835-, 2007, pp. 835–839.
[6] Z.W. Wang, H.M. Wu, Dynamic analysis and simulation of a top loaded washing machine, *China Mechanical Engineering* 13 (23) (2002) 2033–2035.
[7] K. Green, A.R. Champneys, N.J. Lieven, Bifurcation analysis of an automatic dynamic balancing mechanism for eccentric rotors, *Journal of Sound and Vibration* 291 (2006) 861–881.
[8] J. Guckenheimer, P. Holmes, *Nonlinear Oscillations Dynamical Systems and Bifurcations of Vector Fields*, Springer, Berlin, 1983.